PROCEEDINGS OF SCIENCE

Low-Cost CMOS Tech for Inclusive High-Energy Physics Education

L. Barreiro,[a] **S. Benas,**[a,b] **C. Bonifazi,**[c] **A. M. Botti,**[d] **F. Cammarata,**[a] **M. Danussi,**[a] **E. Depaoli,**[a,e] **P. López Maggi,**[a] **J. Pérez Lanzillotta,**[a] **D. Rodrigues,**[a,b] **G. Schulze**[a] **and J. Tiffenberg**[d]

[a] *Departamento de Física, FCEN, Universidad de Buenos Aires, Argentina.*
[b] *CONICET, Universidad de Buenos Aires, Instituto de Física de Buenos Aires (IFIBA).*
[c] *CBPF-MCTI & ICIFI-UNSAM*
[d] *Fermi National Accelerator Laboratory, PO Box 500, Batavia IL, 60510, USA*
[e] *Comisión Nacional de Energía Atómica, Centro Atómico Constituyentes*

E-mail: lara7barreiro@gmail.com

We present a comprehensive characterization of commercial CMOS sensors using complementary measurement techniques. We focus on obtaining the Photon Transfer Curve, Dark Current, and Read Noise as key performance parameters. The Photon Transfer Curve was derived to evaluate the sensor's dynamic range and linearity. This was accomplished using two different methods: the conventional approach, based on homogeneous images, and a novel complementary method, which relies on repeated samples of the same inhomogeneous image. Additionally, we studied the temperature dependence of dark current, taking into account the effect of an infrared filter, and the readout noise was determined as low as 2 electron per pixel. This work establishes the technical foundation for characterizing and operating CMOS sensors, serving as a starting point for a series of undergraduate experiments. Nevertheless, it also offers valuable insights into the operational limits and potential scientific applications of commercial CMOS sensors.

39th International Cosmic Ray Conference (ICRC2025)
15–24 July 2025
Geneva, Switzerland

PoS(ICRC2025)1239

1. CMOS cameras

CMOS (Complementary Metal-Oxide-Semiconductor) cameras are one of the most popular imaging technologies today, primarily due to their low cost, compact size, and versatility. CMOS are pixeled silicon detectors that detect light through the internal photoelectric effect. This technology has drastically improved over the past two decades [1, 2], which led to their implementation in numerous fields, ranging from smartphone cameras to scientific applications such as space astronomy and particle detection [3–6].

CMOS cameras use Bayer filters to reconstruct colored images, consisting of an array of red, green, and blue filters. This filter pattern is arranged with twice as many green pixels as red and blue, reflecting human vision's greater sensitivity to green light. The filter is placed over the sensor's pixels, allowing each pixel to capture only one color. Algorithms known as demosaicing algorithms then combine this color information to produce a full-color image. In addition, CMOS cameras implement an infrared filter that blocks lower-energy photons to avoid distortion and conserve image quality.

In this work, we characterize a Raspberry Pi High-Quality Camera, which consists of a Sony IMX477 CMOS [7] back-illuminated sensor package for easy implementation with a Raspberry Pi. It features a (3040×4056) pixels with a pixel size of $1.55\,\mu$m. Then, each camera has 1520×2028 red and blue pixels, and $2 \times 1520 \times 2028$ green. Contrary to most off-the-shelf CMOS sensors, the Sony IMX477 allows capturing the pixel raw signal, bypassing on-chip processing, such as demosaicing, compression, or noise reduction, and preserving the original intensity. This feature facilitates measuring the sensor key parameters such as dark current, gain, and readout noise, which are otherwise inaccessible.

The remainder of this work is organized as follows. In Section 2, we describe two calibration methods based on the Photon Transfer Curve of the CMOS. In Section 3, we present results on the readout noise and dark current. Finally, in Section 4, we summarize and discuss the potential applications of these sensors.

2. Photon transfer curves

The complementary methods used in this work rely on the statistics of the number of charges, q, generated in each pixel, either due to incident radiation (*e.g.* light) on the sensor or internal charge production mechanisms (*e.g.* dark current). Given the large number of pixels and the low probability of these processes occurring in any single one, the occupancy per pixel is well described by a Poisson distribution.

Under this assumption, the variance of the charge in electrons $Var(Q_e)$ is equal to the expectation value $E(Q_e)$; however, since the charge is measured in Analog-to-Digital Units (ADU), the relationship between them becomes

$$Var(g\,Q_e) = E(g\,Q_e) \Rightarrow g\,Var(Q_{ADU}) = E(Q_{ADU}) \tag{1}$$

where the gain g is defined as the conversion factor to translate the charges measured in ADU to e^-.

Therefore, measuring $\mathrm{Var}(Q_{ADU})$ as a function of $E(Q_{ADU})$ for increasing values of Q provides information regarding the sensor's gain over the dynamic range of the occupancy. Such a

curve, known as Photon Transfer Curve (PTC) has been established as an invaluable process for characterizing pixelated sensors and for quantifying performance optimization. It enables the absolute evaluation of various features, such as read noise, dark current, linearity, pixel nonuniformity, and dynamic range, among others [8].

Two different approaches for obtaining the PCT are presented in this work: one uses a set of homogeneous images with increasing occupancy, as described in Section 2.1, and the other examines the variation in the number of charges of each pixel along a stack of several instances of the same image, as described in Section 2.2.

2.1 PTC from Homogeneous Images

Using the fact that the electron charge produced in a single pixel illuminated with a given intensity follows Poisson statistics, we can construct the PTC by uniformly illuminating the sensor and measuring the variance and mean of the resulting homogeneous images. Repeating this process across a range of illumination intensities allows us to characterize the sensor's response over its full dynamic range, as shown in Eq. 1.

To perform the measurements with homogeneous white light, we used an RGB screen to illuminate the CMOS sensor. Both elements were controlled from the same Raspberry Pi 4, and the entire system was set up in a dark room. We saved the images in RAW format to avoid any kind of gamma correction or internal processing that could affect the linearity of the measured signal. We set an exposure time of 30 seconds, within which the screen was turned on for a few seconds. The reason for keeping the screen off during the sensor readout is to avoid the appearance of stripes in the image, caused by the sensor's readout process and the screen's refresh rate.

To sweep through different intensities, we varied both the screen's on-time (1 to 24 seconds) and the number of lit pixels, adjusting the size of a central square so that the illuminated fraction ranged from 4% to 25%. Here, we swept through the entire possible range of intensities for each of the color channels of the pixels, attempting to reach the saturation point. This procedure covered 60 different intensities from 0 to 4095 ADUs (the full dynamic range of the sensor), taking a single image for each intensity.

Before constructing the PTC, it was essential to ensure that the illumination on the sensor is truly homogeneous. To do so, we take advantage of the statistical properties of the charge collected in each pixel. Under homogeneous illumination, all pixels sample the same Poisson distribution, meaning they can be treated as independent realizations of the same random variable. However, if the mean number of electrons is large enough, the Poisson distribution becomes approximately Gaussian, as guaranteed by the Central Limit Theorem. Based on this, we convert the charge histograms from ADUs to units of electrons using a range of plausible gain factors. For each conversion, we fit the resulting distribution with a Gaussian curve. Since both the mean and variance are free parameters in the fit, the best-fit Gaussian will typically show different values for each. However, the correct gain factor should yield a distribution where the fitted mean and variance are equal, underlying the Poisson nature of the data.

As shown in Fig. 1**a**, we performed Gaussian fits on the converted distributions for a range of possible gain values and compared their respective means and variances. After identifying the gain that results in both having matching values, we verify that, for this factor, the converted distribution can be correctly fitted by a Poisson curve (Fig. 1**b**). Moreover, comparing the fit for this gain factor

to those for bigger and smaller factors illustrates how, for these two cases, the Poisson curves fail to properly capture the width of the resulting distributions.

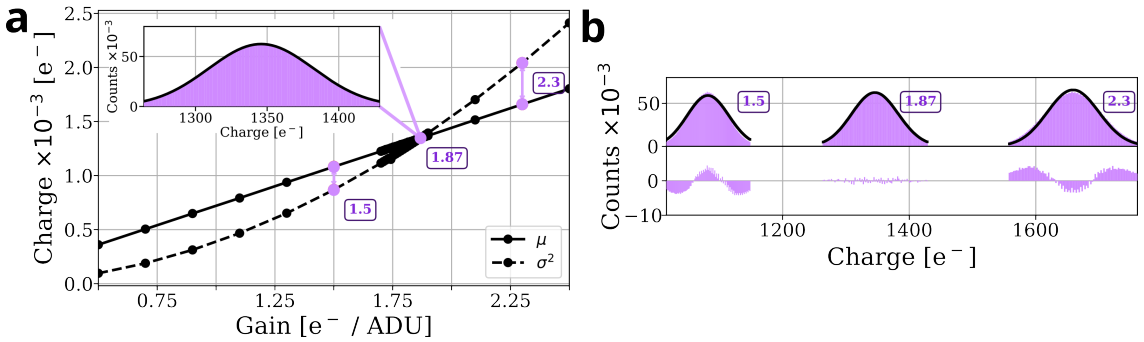

Figure 1: (a) Mean μ and variance σ^2 of the Gaussian fits for the charge distribution as a function of the gain factor. The intersection between both curves identifies the correct gain factor (whose corresponding charge distribution and fit are also shown), and gain values on either side are highlighted. (b) Poisson fits for the charge distributions corresponding to the three highlighted gain factors.

For each illumination level, we calculate the mean and variance of the charge in the pixels across the image for each color. Using this data, we construct the PTC shown in Fig. 2. Each point in the plot corresponds to a single image and represents a statistic based on approximately three million data points, corresponding to the number of pixels of the same color on the sensor. The curves exhibit a nonlinear behavior, suggesting that the conversion factor g may depend on occupancy. This nonlinearity likely arises during the readout process and is probably due to the readout transistor or the electronics, rather than the pixels themselves. Producing homogeneous images is particularly challenging when using low-cost equipment, as is often the case in educational settings or in resource-limited contexts. This lack of homogeneity introduces additional variance into the measurements, which leads to an underestimation of the gain.

2.2 PTC from inhomogeneous Images

In Section 2.1 we performed the PTC curve by means of the ratio between the variance and mean of charge in homogeneous images. Here, we used a different approach, which consisted of

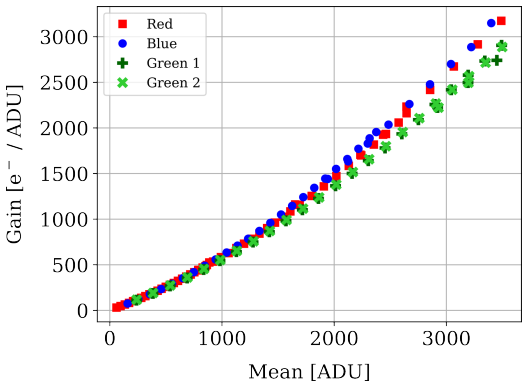

Figure 2: Photon Transfer Curve from homogeneous image using white ligeht.

obtaining the PTC by analyzing the *history* of a single pixel across several images of the same non-homogeneous picture. Averaging multiple images is a common background subtraction technique in image processing [9], and in this context, it also helps reduce temporal noise, allowing for a more accurate estimation of the pixel's standard deviation.

This approach enables us to analyze a range of occupancy levels within a single image, as it contains regions with high and low illumination. For this purpose, we acquired a set of 60 identical images, each taken with an exposure time of 1 second. We were thus able to study the history of the same pixel in different images. By performing statistics on each pixel separately, we constructed their respective variance and mean matrices, shown in Fig. 3. Additionally, in panel **c** we compare the mean and the variance values obtained with both methods. These values are not calculated for the other plots, since only red colors (indicating low occupancy) are available, as shown in Fig. 2. Even though the two methods do not yield exactly the same result, they are compatible for certain occupancy ranges. Nonetheless, the inhomogeneous method is considered more reliable, given that it is difficult to generate truly homogeneous images using a low-cost setup.

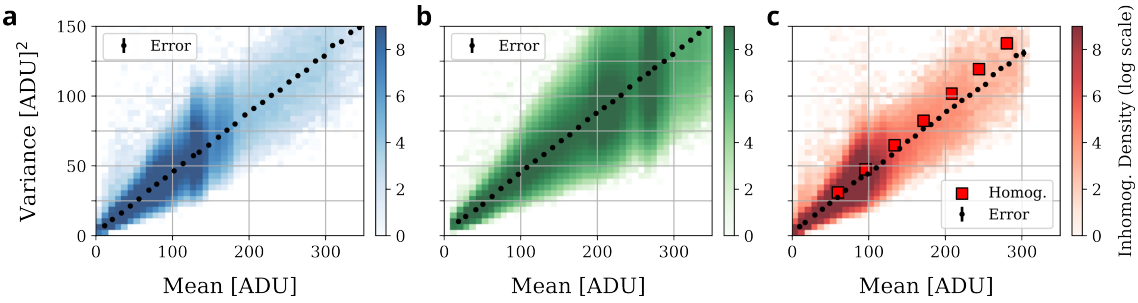

Figure 3: Variance as a function of the mean for the colors: (a) blue, (b) a single green channel and (c) red. For comparison, we include the mean and variance obtained using homogeneous images.

We analyzed the gain per pixel, separating the data by color and distinguishing between the two green subpixels. From these results, we built the gain histograms for the four color channels, shown in Fig. 4. We then compared the normalized histograms of the gain for the three different colors in the Bayer filter, obtaining an average gain of $g = (2.36 \pm 0.01)$ e$^-$/ADU. This result confirms the internal consistency of our method and highlights the robustness of the gain estimation across all color channels, indicating that this approach is less sensitive to inhomogeneities.

3. Readout noise and Dark current characterization

Readout noise can be determined as the standard deviation of the charge in images taken with zero exposure time. To measure this, we captured twenty images under controlled conditions and calculated the standard deviation for each one. By averaging these deviations, we determined the electronic read noise to be $\sigma_e = (3.06 \pm 0.01)$ e$^-$.

Another internal contribution is dark current, which arises from thermal fluctuations within the sensor that moves electrons from the valence to the conduction band [10]. Just like the charge caused by exposure to a light source, the charge from dark current also follows a Poisson distribution and depends on the sensor's exposure time (Δt) and temperature. In this Section, all

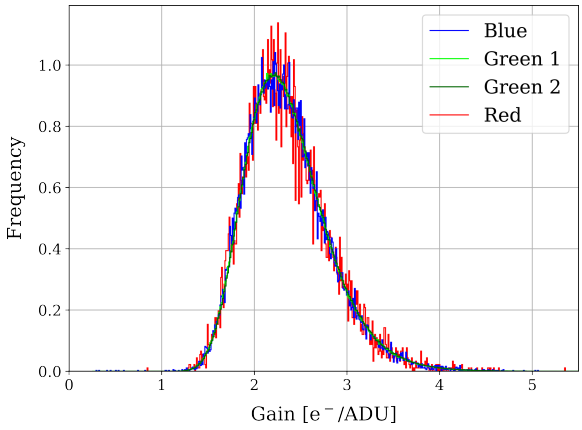

Figure 4: Gain histogram for the four color channels.

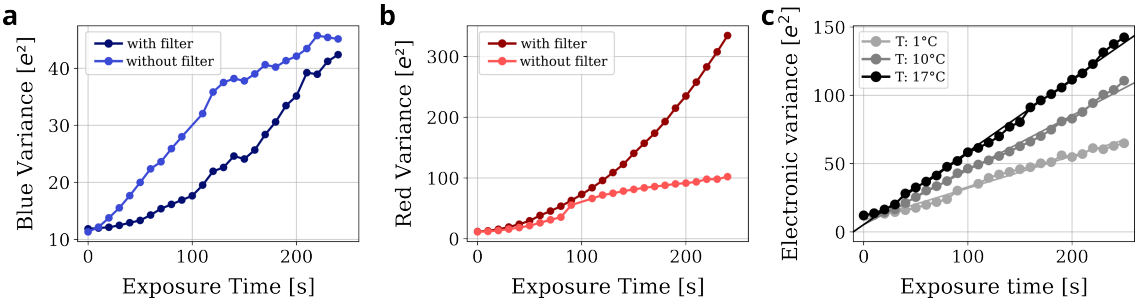

Figure 5: (a–b) Electronic variance as a function of exposure time at a controlled temperature of 1 °C for blue and red pixels, respectively (c) Electronic variance of dark current for three controlled temperatures, without the infrared filter.

variances were converted from ADUs to electrons using the gain obtained with the inhomogeneous method described in Section 2.2.

Since the pixel population can be estimated by the mean, and this mean equals the variance due to the Poisson distribution, the dark current rate, η_{DC}, can be determined as:

$$\eta_{DC} = Var^{DC}(Q_e)/\Delta t. \tag{2}$$

As the Eq 2 is valid only when the sensor is not exposed to an external source, measurements were performed with the sensor shielded by aluminum foil (acting as a Faraday cage) to avoid external contributions and at room temperature (24 °C).

Initial measurements showed a polynomial rather than linear dependence, which we traced to temperature fluctuations and possible emission from the infrared filter. Repeating the experiment inside a temperature-controlled refrigerator and without the filter restored the expected linear behavior, as shown in Fig. 5**a,b**. Additionally, the infrared filter may have emitted radiation within the spectral range it was designed to block, contributing to the observed nonlinearity, predominantly affecting the red pixels. This effect is less pronounced for the blue pixels, which aligns with the fact that red and blue occupy opposite ends of the visible light spectrum.

Finally, Fig. 5**c** shows the electronic variance obtained for three different controlled temperatures (without the infrared filter). We observe qualitatively that the variance increases as the

temperature rises, which is consistent with the thermal origin of this contribution. This linear behavior allowed us to calculate the dark current rate for each temperature, following Eq. (2). The results obtained are presented in Table 1.

Table 1: Dark current rate at different temperatures.

T [°C]	η [e/pix·s]
1	0.235 ± 0.006
10	0.394 ± 0.007
17	0.532 ± 0.007

4. Discussion and conclusion

In this work, we presented a characterization of an off-the-shelf CMOS camera using complementary methods to extract key performance parameters such as gain, dark current, and readout noise. The Photon Transfer Curve (PTC) was successfully obtained through two approaches: one based on homogeneous images and another using repeated captures of an inhomogeneous scene. The second method proved especially valuable in low-cost setups, where achieving uniform illumination is more challenging than high-tech setups. Our results show good consistency between the methods for specific occupancy ranges, validating the inhomogeneous technique as a reliable alternative.

The Sony IMX477 CMOS sensor offers broad potential for both educational and scientific use. It enables hands-on lectures on cutting-edge techniques applied to particle physics, instrumentation, and electronics, and it is widely accessible due to the tool's availability and low cost. Some educational programs may include:

- **Particle detection**: This CMOS camera allows us to see ionization tracks from charged leptons, which we can differentiate by the trace shape.
- **Muon hodoscope**: By stacking two cameras and looking for spatial coincidences in the output images, we can track the passage of muons through the detection region, reconstructing their path and extracting the impinging direction.
- **Minimum ionizing particles in silicon**: The CMOS camera works as a particle detector to measure muon energy deposits; by analyzing the pixel charge we can obtain the energy loss per unit length.
- **X-ray detection**: We can use the CMOS camera to measure X-ray absorption in silicon from a radioactive source. Know the X-ray energy we could obtain the mean electron-hole pair creation energy and fano noise.

This versatility makes commercial CMOS sensors a valuable platform not only for teaching but also for scientific research. Future work could explore the extension of these methods to dynamic scenes or for field applications.

Acknowledgments

We gratefully acknowledge the support of public and high-quality education. We also wish to recognize the prior work by Takano and Hibino, presented at the 38th ICRC, which pioneered the use of CMOS cameras as pocket-sized particle detectors [11].

References

[1] E. R. Fossum, "CMOS image sensors: electronic camera-on-a-chip". *IEEE Transactions on Electron Devices*, vol. 44, no. 10, pp. 1689–1698, 1997. doi:10.1109/16.628824.

[2] A. J. P. Theuwissen, "CMOS Image Sensors: State-of-the-Art Technology, Applications, and Future Trends," *Solid-State Electronics*, vol. 52, no. 9, pp. 1401–1406, 2008. doi:10.1016/j.sse.2008.04.012.

[3] M. Pérez, J. Lipovetzky, M. Sofo Haro, I. Sidelnik, J. J. Blostein, F. Alcalde Bessia, and M. Gómez Berisso, "Particle detection and classification using commercial off-the-shelf CMOS image sensors," *Nuclear Instruments and Methods in Physics Research Section A*, vol. 827, pp. 171–180, 2016. doi:10.1016/j.nima.2016.04.072.

[4] M. Pérez, J. J. Blostein, F. P. Alcalde Bessia, A. Tartaglione, I. P. Sidelnik, M. F. Sofo Haro, S. G. Suárez, M. L. Gimenez, M. Gómez Berisso, and J. Lipovetzky, "Thermal neutron detector based on COTS CMOS imagers and a conversion layer containing Gadolinium," *Nuclear Instruments and Methods in Physics Research Section A*, vol. 893, pp. 157–163, 2018. doi:10.1016/j.nima.2018.03.032.

[5] F. P. Alcalde Bessia, M. Pérez, J. Lipovetzky, N. A. Piunno, H. Mateos, I. P. Sidelnik, J. J. Blostein, M. F. Sofo Haro, and M. Gómez Berisso, "X-ray micrographic imaging system based on COTS CMOS sensors," *International Journal of Circuit Theory and Applications*, vol. 46, no. 10, pp. 1848–1857, 2018. doi:10.1002/cta.2502.

[6] M. Pérez, O. I. Abbate, J. Lipovetzky, F. P. Alcalde Bessia, F. A. Sánchez, M. F. Sofo Haro, J. M. Longhino, M. Gómez Berisso, and J. J. Blostein, "Neutron imaging based on transfer foil activation and COTS CMOS image sensors," *Journal of Instrumentation*, vol. 17, no. 2, P02004, 2022. doi:10.1088/1748-0221/17/02/P02004.

[7] Sony Corporation, "IMX477 Data Sheet" Available at: https://docs.arducam.com/Raspberry-Pi-Camera/Native-camera/source/IMX477-DS.pdf. Accessed: 2025-04-21.

[8] J. R. Janesick, *Scientific Charge-Coupled Devices*, SPIE Press, Bellingham, Washington, 2001. Series: Tutorial Texts in Optical Engineering, vol. TT39. ISBN: 0-8194-3698-4.

[9] Becker, G.S.; Lovas, R. "Uniformity Correction of CMOS Image Sensor Modules for Machine Vision Cameras," *Sensors*, 22, 9733, 2022. doi:10.3390/s22249733

[10] N. W. Ashcroft and N. D. Mermin, *Solid State Physics*, Holt, Rinehart and Winston, 1976. ISBN: 0-03-083993-9.

[11] Takano, Wakiko and Hibino, Kinya, *Consumer Devices with CMOS camera image sensors as Pocket-Sized Particle Detectors*. PoS, 2023, vol. ICRC2023. doi:10.22323/1.444.1620